Laboratory Investigation of Mean Drag in a Random Array of Rigid, Emergent Cylinders

Yukie Tanino[1] and Heidi M. Nepf[2]

Abstract: This paper investigates the drag exerted by randomly distributed, rigid, emergent circular cylinders of uniform diameter d. Laboratory measurements are presented for solid volume fraction $\phi=0.091$, 0.15, 0.20, 0.27, and 0.35 and cylinder Reynolds number $Re_p \equiv U_p d/\nu = 25$ to 685, where U_p=temporally and cross-sectionally averaged pore velocity and ν=kinematic viscosity. These ranges coincide with conditions in aquatic plant canopies. The temporally and cross-sectionally averaged drag coefficient, C_D, decreased with increasing Re_p and increased with increasing ϕ under the flow conditions investigated. The dimensionless ratio of the mean drag per unit cylinder length $\langle \overline{f_D} \rangle_H$ to the product of the viscosity, μ, and U_p exhibits a linear Re_p dependence of the form $\langle \overline{f_D} \rangle_H / (\mu U_p) = \alpha_0 + \alpha_1 Re_p$, consistent with Ergun's formulation for packed columns. In the range of experimental conditions, α_1 increases monotonically with ϕ. In contrast, α_0 is constant within uncertainty for $0.15 \leqslant \phi \leqslant 0.35$, which suggests that viscous drag per unit cylinder length is independent of ϕ in this range.

DOI: 10.1061/(ASCE)0733-9429(2008)134:1(34)

CE Database subject headings: Vegetation; Drag; Aquatic plants; Two-dimensional flow; Open channel flow; Experimental data; Cylinders.

Introduction

Aquatic vegetation alters its environment in many ways. Most important, plants introduce additional hydraulic resistance to the flow, which may significantly reduce the volumetric flow rate in channels. Vegetation also influences the transport of dissolved and particulate material. For example, plant stems enhance lateral dispersion by forcing solute to follow tortuous trajectories and by enhancing turbulence intensity (Nepf et al. 1997; Tanino and Nepf, private communication, 2007). In addition, suspended sediment transport is reduced in channels with submerged vegetation because of the reduction in bed shear stress (López and García 1998). Similarly, treatment wetlands have been observed to reduce the total suspended solid concentration by as much as 90% (Knight et al. 1999), demonstrating that vegetation can create conditions favorable to particle removal.

The impact of vegetation is largely determined by the additional drag it provides, which can be characterized by a temporally and spatially averaged drag coefficient, defined here as

$$C_D \equiv \frac{\langle \overline{f_D} \rangle}{\rho \langle \overline{u} \rangle^2 \langle d \rangle / 2} \tag{1}$$

where $\langle \overline{f_D} \rangle$=average drag in the direction of the average flow per unit length of stem; ρ=fluid density; $\langle d \rangle$=characteristic plant width (i.e., the dimension perpendicular to the mean flow); and $\langle \overline{u} \rangle$=fluid velocity in the direction of the mean flow averaged over the pore space between stems. Specifically, $\langle \overline{f_D} \rangle$, $\langle \overline{u} \rangle$, and $\langle d \rangle$ are averages over a time interval much longer than time scales associated with turbulent fluctuations and vortex shedding (denoted by an overbar) and over a volume that spans many plants (denoted by angular brackets). In addition to describing the mean drag exerted by the vegetation, C_D is also required in models for turbulence intensity (Nepf 1999) and longitudinal dispersion (White and Nepf 2003) in plant canopies.

An aquatic plant stem is often modeled as a circular cylinder of uniform diameter d. The drag coefficient of an isolated cylinder is well established. In particular, C_D decreases with increasing Reynolds number, $Re_p \equiv \langle \overline{u} \rangle d/\nu$, up to $Re_p = O(10^3)$, where ν=kinematic viscosity. C_D is also influenced by the presence and relative position of neighboring cylinders. For example, a cylinder in the wake of an upstream cylinder experiences a velocity deficit relative to $\langle \overline{u} \rangle$. Consequently, the downstream cylinder experiences a reduced drag (Blevins 2005; Zdravkovich and Pridden 1977; Petryk 1969). Petryk (1969) investigated the influence of a neighboring cylinder on the drag measured at a test cylinder. His data show that, when the cylinders are sufficiently close, the mean drag on the pair of cylinders could be either smaller or greater than that for an isolated cylinder depending on the orientation of the cylinders. In a random array, both the distance between and the relative orientation of each cylinder and its neighbors differ for each cylinder, and it is not obvious whether the array-averaged C_D, as defined by Eq. (1), is enhanced or reduced relative to an isolated cylinder.

If plant stems are modeled as randomly distributed, rigid, cir-

[1]Research Assistant, Ph.D. Candidate, Dept. of Civil and Environmental Engineering, Massachusetts Institute of Technology, 77 Massachusetts Ave. 48-216-24, Cambridge, MA 02139. E-mail: ytanino@alum.mit.edu

[2]Professor, Dept. of Civil and Environmental Engineering, Massachusetts Institute of Technology, 77 Massachusetts Ave. 48-216D, Cambridge, MA 02139. E-mail: hmnepf@mit.edu

Note. Discussion open until June 1, 2008. Separate discussions must be submitted for individual papers. To extend the closing date by one month, a written request must be filed with the ASCE Managing Editor. The manuscript for this paper was submitted for review and possible publication on January 30, 2007; approved on June 22, 2007. This paper is part of the ***Journal of Hydraulic Engineering***, Vol. 134, No. 1, January 1, 2008. ©ASCE, ISSN 0733-9429/2008/1-34–41/$25.00.

Table 1. Summary of Studies That Collected Drag Data in Emergent Arrays

Source	Array	Configuration	ϕ	Reynolds number
Ayaz and Pedley 1999	Rigid cylinders (N)	Square	0.13	$\leqslant 40.00/(1-\phi)$
			0.35	
			0.50	
			0.59	
Koch and Ladd 1997	Rigid cylinders (N)	Random	0.05	$\leqslant 37$
			0.10	$\leqslant 33$
			0.20	$\leqslant 100$
			0.40	$\leqslant 67$
		Square, staggered	0.2	57–210
			0.4	82–320
Lee et al. 2004	Sawgrass (L; F)	N/A	N/A	0–200 (L)
				$70-10^4$ based on depth (F)
Mazda et al. 1997	Two tidal mangrove swamps (F)	N/A	0.05–0.45 (depth dependent)	N/A
Nepf 1999	Rigid cylinders (L)	Random	0.006	4,000–10,000
			0.02	
			0.06	
Petryk 1969	Rigid cylinders (L)	Random	0.015	$(0.6-5)\times 10^4$
			0.027	$(3-9)\times 10^4$
Stone and Shen 2002	Rigid cylinders (L)	Staggered	0.0055	$O(250-8{,}000)$ assuming
			0.0220	$\nu = 0.009$ cm^2/s
			0.0610	
Wu et al. 1999	Flexible horsehair mattress (L)	N/A	N/A	20–3,000 based on depth and $U_p(1-\phi)$

Note: In the second and fifth columns, (N), (F), and (L) indicate numerical, field, and laboratory results, respectively. N/A denotes information not available or not applicable. Cylinders are circular. Reynolds numbers are based on the cylinder diameter d and U_p unless otherwise noted. The Reynolds number for Lee et al.'s (2004) measurements is defined using the depth average of the spatially averaged width of all stems and leaves as the length scale.

cular cylinders, the cylinder configuration can be characterized in a spatially averaged sense by the solid volume fraction, ϕ, and d. Then, C_D is expected to be a function of ϕ, d, and Re_p. The present study considers only the Re_p and ϕ dependence. In salt marshes, stem diameter $\langle d\rangle = 0.2-1.2$ cm, $\phi = 0.001-0.02$, and local flow speeds of the range 0–10 cm/s have been reported (Valiela et al. 1978; Leonard and Luther 1995). In contrast, ϕ as high as 0.45 and mean trunk diameters of $\langle d\rangle = 4-9$ cm have been reported in mangroves (Mazda et al. 1997; Furukawa et al. 1997). Local flow speeds of the range 0–5 cm/s have been observed 15 m (Kobashi and Mazda 2005) and 120 m (Mazda et al. 1997) from the interface between the mangrove and a river. Finally, constructed wetlands may be as dense as $\phi = 0.65$ (Serra et al. 2004). These values suggest that field conditions span $Re_p = 0$ to $O(4{,}000)$ and $\phi = 0-0.65$.

Although many recent studies have investigated drag in real and model canopies (see Table 1 for examples), a comprehensive data set is not yet available for the entire range of conditions expected in emergent aquatic plant canopies. Specifically, for the simple two-dimensional array of randomly distributed cylinders, data are not available at $\phi > 0.05$ for $Re_p > 100$ or $\phi < 0.05$ at $Re_p < 1{,}000$. Moreover, previous studies have reported contradictory ϕ dependence for C_D. Nepf's (1999) numerical model, which considers two-cylinder interactions in a random array, predicts a monotonically decreasing C_D with increasing ϕ for $8\times 10^{-4} < \phi < 0.24$ (Nepf 1999, Fig. 6). Nepf (1999) verified this model with laboratory measurements at $Re_p \geqslant 1{,}000$. Similarly, Lee et al. [(2004), Eq. (18)] proposed that the depth-averaged C_D is inversely proportional to the depth-averaged frontal area per unit volume and characteristic spacing of all stems and leaves. However, these dependencies were not explicitly investigated in that paper. In contrast, C_D increases with ϕ for $Re_p \leqslant O(100)$ in Koch and Ladd's (1997) numerical simulations of random arrays for $\phi = 0.05-0.4$.

This paper presents laboratory measurements of the depth-averaged C_D in random arrays of rigid emergent cylinders of $\phi = 0.091-0.35$ and $Re_p = 25-685$, where Re_p was calculated using the mean pore velocity, U_p, which is the cross-sectional average of $\langle\bar{u}\rangle$. The Re_p dependence of the depth-averaged $\langle\overline{f_D}\rangle$ is compared with Ergun's (1952) equation, and the coefficients in that equation are determined for each ϕ. The results are compared with Koch and Ladd's (1997) numerical simulations and Petryk's (1969) laboratory measurements.

Theory

We consider an array of rigid circular cylinders of uniform diameter d distributed randomly with a constant density m (cylinders per unit horizontal area). The corresponding solid volume fraction is $\phi = m\pi d^2/4$. The Cartesian coordinates $\mathbf{x} \equiv (x,y,z) \equiv (x_1,x_2,x_3)$ are defined with the x-axis aligned with U_p and the y-axis perpendicular to it in the horizontal plane. The z-axis is positive upwards, with $z=0$ at the horizontal bed.

Following the standard formulation in terrestrial canopy literature, e.g., Finnigan (2000), the pressure $p(t,\mathbf{x})$ and velocity $\mathbf{v}(t,\mathbf{x}) \equiv (u,v,w) \equiv (u_1,u_2,u_3)$ are first decomposed into the local time average $(\overline{u_i},\overline{p})$ and instantaneous deviations from it (u_i',p'), where $\overline{u_i'},\overline{p'} = 0$. Then, the temporally averaged quantities are further decomposed into their spatial average $(\langle\overline{u_i}\rangle,\langle\overline{p}\rangle)$ and deviations from that average $(\overline{u_i}'',\overline{p}'')$, where $\langle\overline{u_i}''\rangle,\langle\overline{p}''\rangle = 0$. The overbar

denotes a temporal average over an interval much longer than the time scales of vortex shedding and turbulent fluctuations and angular brackets denote a spatial average over an infinitesimally thin volume V_f that spans many cylinders but excludes all solid volume (see, e.g., Finnigan 1985, 2000). Recall that the array is homogeneous. The water depth $H(t,\mathbf{x})$ is also decomposed analogously. $\langle \bar{H} \rangle \gg |\bar{H}''|, |H'|$ in systems considered in this paper. Applying the same temporal and spatial averaging operations to the governing equations yields ($i, j=1, 2, 3$)

$$\frac{\partial \langle \bar{u}_i \rangle}{\partial t} + \langle \bar{u}_j \rangle \frac{\partial \langle \bar{u}_i \rangle}{\partial x_j} = g_i - \frac{1}{\rho}\frac{\partial \langle \bar{p} \rangle}{\partial x_i} - \frac{\partial \langle \overline{u_i' u_j'} \rangle}{\partial x_j} + \nu \frac{\partial}{\partial x_j}\frac{\partial}{\partial x_j}\langle \bar{u}_i \rangle - \frac{\partial \langle \bar{u}_i'' \bar{u}_j'' \rangle}{\partial x_j} - f_i \tag{2}$$

where $g_i = i$th component of the gravitational acceleration and

$$f_i = -\frac{\nu}{V_f}\int\int_{S_c} \frac{\partial \bar{u}_i}{\partial n} dS + \frac{1}{\rho V_f}\int\int_{S_c} \bar{p} n_i dS \tag{3}$$

is the net hydrodynamic force per unit fluid mass exerted on S_c, where S_c denotes all cylinder surfaces that intersect V_f and $\mathbf{n}$=unit normal vector on S_c pointing out of V_f. f_1 represents the net cylinder drag per unit fluid mass from which $\langle \bar{f}_D \rangle$ in Eq. (1) can be calculated: $\langle \bar{f}_D \rangle = \rho(1-\phi) f_1/m$. The third and fifth terms on the right-hand side of Eq. (2) are the divergence of the spatially averaged Reynolds stress and the dispersive stress, respectively. The latter arises from spatial correlations of the local deviations from the temporally and spatially averaged velocity.

Ergun (1952) proposed an expression for pressure drop in packed columns which, when rearranged, yields the dimensionless drag parameter

$$\frac{\langle \bar{f}_D \rangle}{\mu \langle \bar{u} \rangle} = \alpha_0 + \alpha_1 Re_p \tag{4}$$

where μ=viscosity; α_0 is a function of ϕ; and α_1 is a constant. Substituting Eq. (4) into Eq. (1) yields the corresponding relationship for C_D:

$$C_D = 2\left(\frac{\alpha_0}{Re_p} + \alpha_1\right) \tag{5}$$

The first term in Eqs. (4) and (5) describes the viscous contribution that arises from the viscous shear stress on the cylinder surface, which corresponds to the first term in Eq. (3). The second term in Eqs. (4) and (5) describes the inertial contribution arising from the pressure loss in the cylinder wake, which corresponds to the second term in Eq. (3). Koch and Ladd (1997) show for arrays of $\phi = 0.05-0.4$ that cylinder drag may also be described by a linear Re_p dependence of the same form as Eq. (4), but with both α_0 and α_1 varying with ϕ. Also, C_D of a smooth isolated cylinder is described by the empirical expression (White 1991, p. 183),

$$C_D \approx 1 + 10.0 Re_p^{-2/3}, \quad 1 < Re_p < 10^5 \tag{6}$$

which corresponds to [from Eq. (1)]

$$\frac{\langle \bar{f}_D \rangle}{\mu \langle \bar{u} \rangle} \approx 5.00 Re_p^{1/3} + \frac{1}{2} Re_p, \quad 1 < Re_p < 10^5 \tag{7}$$

As Re_p increases, the second term becomes increasingly large relative to the first term and Eq. (7) approaches a linear Re_p dependence of the form Eq. (4).

In the present laboratory conditions and under certain field conditions, Eq. (2) can be simplified. Here, we consider a two-dimensional, homogeneous array and assume $\langle \bar{v} \rangle = 0$ and $\partial \langle \rangle / \partial y = 0$. Accordingly, the depth average is equivalent to a cross-sectional average. The flow is also steady, $\partial / \partial t = 0$. The free surface gradient ranged in magnitude from 4×10^{-4} to 5×10^{-2} in the cases analyzed, indicating that the vertical length scale $\langle \bar{H} \rangle$ was significantly smaller than the horizontal length scale $\langle \bar{H} \rangle / (d\langle \bar{H} \rangle / dx)$. Under these conditions, Eq. (2) reduces to

$$\langle \bar{u} \rangle \frac{\partial \langle \bar{u} \rangle}{\partial x} + \langle \bar{w} \rangle \frac{\partial \langle \bar{u} \rangle}{\partial z} = -\frac{1}{\rho}\frac{\partial \langle \bar{p} \rangle}{\partial x} - \left(\frac{\partial \langle \overline{u'u'} \rangle}{\partial x} + \frac{\partial \langle \overline{u'w'} \rangle}{\partial z} \right) + \nu \frac{\partial^2 \langle \bar{u} \rangle}{\partial z^2} - \left(\frac{\partial \langle \bar{u}'' \bar{u}'' \rangle}{\partial x} + \frac{\partial \langle \bar{u}'' \bar{w}'' \rangle}{\partial z} \right) - f_1 \tag{8}$$

in the x-direction. Recall that the bed is horizontal, i.e., $g_1 = g_2 = 0$ and $g_3 = -g$. We also assume that the $i=3$ component of Eq. (2) reduces to the hydrostatic pressure balance. White (2002) measured velocity in random arrays of $\phi = 0.010-0.063$. From his measurements closest to the bed, where $\overline{w'w'}$ varied most rapidly with depth, $\overline{w'^2}/z$ ranged from 0.007 to 6.5 cm/s^2 ($\ll |g_3|$). These data support the hydrostatic pressure assumption. $\bar{u}''$ is expected to vary on the scale of the cylinder spacing and $\bar{w}''$ on the scale of the water depth and, consequently, correlations between time-averaged spatial deviations are expected to be negligible, i.e., $\langle \bar{u}'' \bar{w}'' \rangle \ll \langle \overline{u'w'} \rangle$ (Kaimal and Finnigan 1994, p. 85). This was verified experimentally for submerged periodic arrays at $\phi = 0.0008-0.013$ (Poggi et al. 2004). In addition, Tsujimoto et al. (1992) measured zero $\overline{u'w'}$ over the entire water column in an emergent periodic array of $\phi = 0.0044$ and 0.0079. Following the above discussion, the third and the sixth terms on the right-hand side of Eq. (8) are neglected.

Next, Eq. (8) is averaged over the water depth. Free surface stress is negligible in the laboratory. Bed shear stress estimated from White's (2002) measurements in a random array of $\phi = 0.010-0.063$ is 0.2–13% of the cylinder drag contribution estimated from the isolated cylinder solution (7). Moreover, the drag contribution from the cylinders is expected to become more dominant as ϕ increases. It should be noted that bed and free surface stresses may be significant in the field, where the bed is typically rough and wind may be non-negligible. Finally, we assume that flow conditions are fully developed, and $\partial \langle \bar{H} \rangle / \partial x$ is only retained to describe the pressure gradient. This is consistent with the horizontally homogeneous array. We thus obtain the balance between the total cylinder drag per unit volume of array and the longitudinal pressure gradient:

$$\langle \bar{f}_D \rangle_H m = -(1-\phi)\rho g \frac{d\eta}{dx} \tag{9}$$

where $\eta(x)$=temporally and spatially averaged displacement of the free surface from the still water level (Fig. 2) and $\langle \bar{f}_D \rangle_H$=depth-averaged $\langle \bar{f}_D \rangle$. Eqs. (1) and (9) yield the following expression for the depth-averaged drag coefficient:

$$\frac{C_D \langle \bar{u} \rangle_H^2}{2} md = -(1-\phi) g \frac{d\eta}{dx} \tag{10}$$

where $\langle \bar{u} \rangle_H$=depth-averaged $\langle \bar{u} \rangle$. By definition, $md = \phi/(\pi d/4)$, and Eq. (10) relates C_D with $d\eta/dx$ for a given ϕ, d, and $\langle \bar{u} \rangle_H$. Where Eq. (10) is valid, Manning's coefficient n_M is related to C_D as

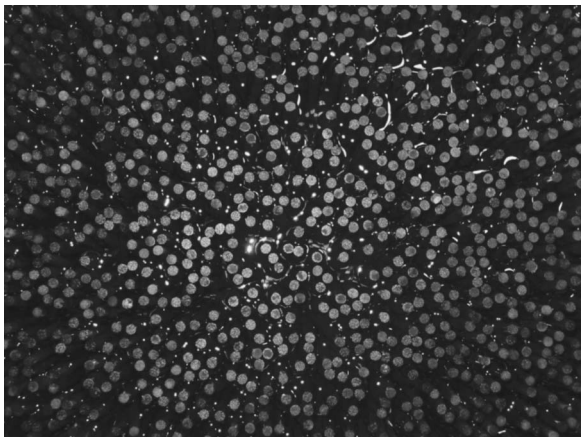

Fig. 1. A section of the $\phi=0.27$ array in plan view

$$n_M = \frac{R^{2/3}}{(1-\phi)^{3/2}}\sqrt{\frac{C_D}{2g}md} \tag{11}$$

where R=hydraulic radius.

Experimental Procedure

Laboratory experiments were performed in two Plexiglas recirculating flumes. Tank A, with a working section of 284 cm $\times$40 cm$\times$43 cm, was used for $\phi=0.15$, 0.20, 0.27, and 0.35 and Tank B, with a working section of 670 cm$\times$20.3 cm$\times$30.5 cm, was used for $\phi=0.091$. In each flume, the volumetric flow rate Q was measured with an in-line flow meter.

Cylindrical maple dowels of diameter $d=0.64$ cm (Saunders Brothers, Inc., Greenwood, Maine) were used as laboratory models for vegetation. The dowels were inserted into four 71.1 cm $\times$40.0 cm custom-made PVC sheets of either $\phi=0.20$ or 0.35 hole fraction to create a 284 cm long array that spanned the flume width. The PVC sheets were created by generating uniformly distributed random coordinates for the hole centers until the desired number of nonoverlapping holes were assigned. Here, nonoverlapping holes were defined to not have any other hole center fall within a $2d\times2d$ square around its center. The $\phi=0.20$ and 0.35 arrays were created by completely filling these sheets, and the $\phi=0.091$, 0.15, and 0.27 arrays were created by partially filling the sheets. For the latter arrays, the holes that were filled were selected by MATLAB's (The MathWorks, Inc.) random number generator. Fig. 1 is a plan view of the $\phi=0.27$ array.

$\eta(x)$ was measured using two sets of surface displacement gauges. The gauges were positioned a longitudinal distance L apart inside the array, with each set attached to a vertical traverse (Fig. 2). Each set consisted of two or three gauges that were distributed laterally across the width of the flume. Each gauge outputs voltage proportional to its submerged length. The signal was amplified before it was sent to the computer to be collected with the acoustic Doppler velocimeter (ADV) data acquisition software ADVA.exe version 4.4 by SonTek, Inc. Measurements from all displacement gauges were simultaneously recorded and time averaged to yield a mean voltage value for each gauge.

After steady conditions were achieved, voltage measurements were recorded over 5–20 min. The surface displacement from the still water level for the jth gauge was determined from the time average of the voltage record at that gauge, V_{f_j}:

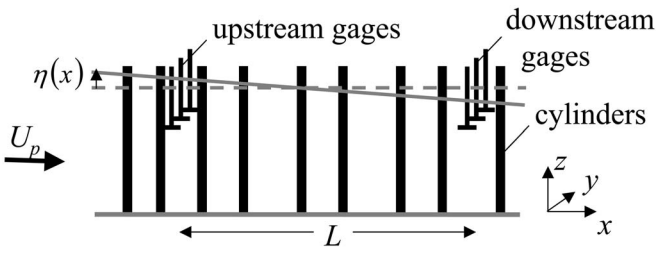

Fig. 2. A section of the cylinder array. Surface displacement gauges were placed a distance L apart longitudinally. In the presence of flow, the free surface (solid line) is displaced by vertical distance $\eta(x)$ from the still water level (dashed line) and a negative free surface gradient develops.

$$\eta_j = \frac{V_{f_j} - V_{0_j}}{(dV/dz)_j} \tag{12}$$

V_{0_j}=time-averaged voltage reading at the jth gauge in still water. $(dV/dz)_j$=gradient of the linear regression of the calibration data for the jth gauge. The local time-averaged water depth at each displacement gauge was $\bar{H}_j=H_{\mathrm{SWL}}+\eta_j$, where $z=H_{\mathrm{SWL}}$ is the still water level. The mean water depth between the displacement gauges, $\langle\bar{H}\rangle_L$, was estimated as the average of the mean $\bar{H}_j$ at the upstream gauges and the downstream gauges. In the present experiments, $\langle\bar{H}\rangle_L$ ranged from 10.0 to 21.8 cm. The gradient of the free surface, $d\eta/dx$, was estimated by calculating the mean of η_j measured by the downstream gauges and the mean of η_j measured by the upstream gauges, subtracting the latter from the former, and dividing the result by L. The cross-sectionally averaged pore velocity between the gauges was estimated as $U_p=Q/(\langle\bar{H}\rangle_L W(1-\phi))$, where W=width of the flume. In the present study, $\langle\bar{u}\rangle_H$ is approximated by U_p. Similarly, the Reynolds number was calculated as $Re_p\equiv U_p d/\nu$. Finally, $\langle\overline{f_D}\rangle_H/(\mu U_p)$ and C_D were determined by substituting the values for U_p and $d\eta/dx$ into Eqs. (9) and (10).

For each experiment, the most conservative estimate of the maximum and minimum C_D was calculated by considering the maximum and minimum $d\eta/dx$ and U_p estimates. The other variables in Eq. (10) do not contribute significantly to the uncertainty. The maximum and minimum $d\eta/dx$ are the gradient of the least-squares fit to data plus and minus its uncertainty, as defined by Taylor (1997, Chap. 8.4). The uncertainty in U_p reflects that of the flow meter reading. Variations in the temperature over the duration of each experiment are also included in the uncertainty for Re_p. In Tank A, a change in temperature was not observed. In Tank B, water temperature increased by as much as 1°C during one time record.

Experimental Results

At low Re_p, small ϕ, or small L, the surface displacement at the gauges was very small, which resulted in large uncertainties or, in some cases, negative C_D estimates. In all subsequent discussion, we exclude all C_D measurements with an uncertainty greater than 25% of the estimated C_D and measurements that are negative within uncertainty. The remaining 120 measurements are discussed in the following. The range of Re_p at each ϕ is provided in Table 2.

J. Hydraul. Eng., 2008, 134(1): 34-41

Table 2. The Coefficients of Eq. (4) Estimated from a Linear Regression on the Present Laboratory Measurements and Petryk's (1969) Laboratory Measurements

Source	ϕ	α_0	α_1	r	n	Re_p range
Petryk 1969	0.015	$(3.0\pm1.2)\times10^3$	0.49±0.04	0.975	10	$(0.6-5)\times10^4$
	0.027	$(3.2\pm2.4)\times10^3$	0.66±0.04	0.993	5	$(3-9)\times10^4$
Present study	0.091	25±12	0.74±0.03	0.985	18	148–685
	0.15	84±14	1.12±0.06	0.969	26	87–396
	0.20	85±5	1.15±0.02	0.996	37	29–482
	0.27	82±2	1.58±0.01	0.999	20	25–294
	0.35	84±6	1.72±0.03	0.997	19	40–305
Koch and Ladd 1997	0.05	11	0.97			5–37
	0.1	17	1.0			6–33
	0.2	40	1.2			6–100
	0.4	167	2.6			8–67

Note: The Re_p range includes only the experimental conditions of the cases that contributed to the linear regression. r=correlation coefficient and n=number of data points included in the regression. The upper and lower estimates for α_0 and α_1 represent the uncertainty in the linear regression estimated from the deviation of $\langle\overline{f_D}\rangle_H/(\mu U_p)$ from the regression, as suggested by Taylor (1997, Chap. 8.4). Also included are α_0 and α_1 extracted from a graphic representation of Koch and Ladd's (1997) numerical results in Koch and Ladd (1997, Fig. 26).

The normalized drag, $\langle\overline{f_D}\rangle_H/(\mu U_p)$, is presented in Fig. 3 as a function of Re_p. $\langle\overline{f_D}\rangle_H/(\mu U_p)$ clearly exhibits a linear dependence on Re_p for all ϕ, consistent with Eq. (4). Moreover, $\langle\overline{f_D}\rangle_H/(\mu U_p)$ at a given Re_p increases with ϕ under the conditions investigated. Fig. 3 also includes the least-squares fits to Koch and Ladd's (1997) simulation results in random cylinder arrays of $\phi=0.05-0.4$ and $5<Re_p<100$ (see Table 2 for numerical values of the coefficients). At $Re_p<100$, $\langle\overline{f_D}\rangle_H/(\mu U_p)$ for $\phi=0.15$, 0.20, 0.27, and 0.35 fall between Koch and Ladd's (1997) $\phi=0.2$ and 0.4 predictions.

The gradient, α_1, and the intercept with the ordinate axis, α_0, of the line of regression of $\langle\overline{f_D}\rangle_H/(\mu U_p)$ on Re_p are presented in Fig. 4. To estimate these coefficients for the isolated cylinder, Eq. (7) was interpolated over $Re_p=148-678$ in increments of 10. A linear regression on these interpolated values yields a correlation coefficient $r=1.000$ ($n=54$) and the coefficients $\alpha_0=23.5\pm0.2$ and $\alpha_1=0.5318\pm6\times10^{-4}$. The Re_p range selected here coincides with that for which α_0 and α_1 were determined for $\phi=0.091$ (Table 2). As the Re_p range over which the linear regression is applied increases, α_0 increases and α_1 approaches 0.50. This sensitivity to Re_p reflects the deviation of Eq. (7) from a linear Re_p dependence. Estimated values of the coefficients are included in Table 2.

α_1 increases monotonically with ϕ, which implies that the inertial contribution increases with ϕ at a given Re_p. This depen-

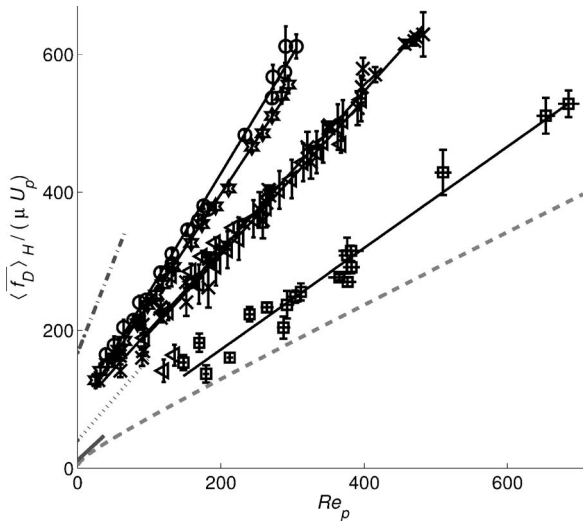

Fig. 3. $\langle\overline{f_D}\rangle_H/(\mu U_p)$ at $\phi=0.091$ (square), 0.15 (left triangle), 0.20 (cross), 0.27 (hexagram), and 0.35 (circle), as defined in Eq. (9). Solid line marks the linear regression for each ϕ. Grey lines represent Koch and Ladd's (1997) numerical results at $\phi=0.05$ (solid line), 0.2 (dotted line), and 0.4 (dash-dotted line), as presented in Table 2. The isolated cylinder solution, Eq. (7), is also presented (grey, dashed line). Horizontal and vertical lines on present data represent the uncertainty in Re_p and C_D, respectively, as described in the text.

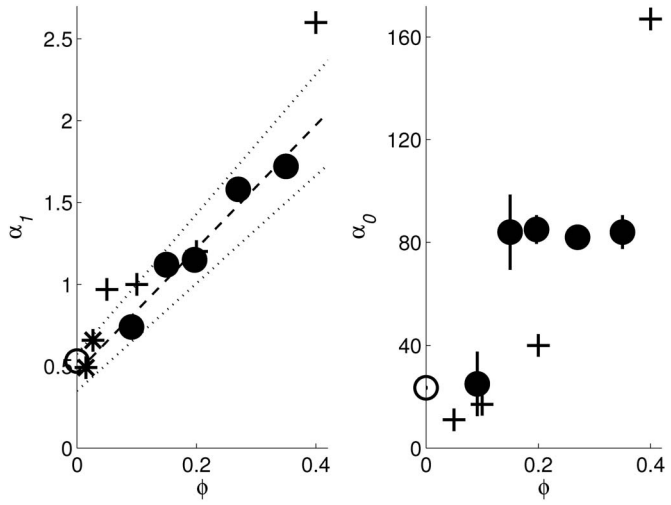

Fig. 4. The coefficients of Eq. (4) estimated from a linear regression on the present laboratory measurements (solid circle), on Petryk's (1969) laboratory measurements (asterisk), on interpolated values of Eq. (7) (open circle), and on Koch and Ladd's (1997) numerical results (plus sign). See Table 2 for numerical values. Vertical bars on present data points and Petryk's (1969) data points represent the uncertainty estimated from the regression, as suggested by Taylor (1997, Chap. 8.4). Where the vertical bars are not visible, they are smaller than the marker size. The dashed and dotted lines are the line of regression of α_1 on ϕ and the associated uncertainty as suggested by Taylor (1997, Chap. 8.4), respectively [Eq. (13)].

dence can be explained as follows. The inertial contribution to $\langle \overline{f_D} \rangle_H$, which arises from the mean pressure drop across the cylinders [Eq. (3)], scales as $\rho d \langle \overline{u}''^2 \rangle_H$. In dimensionless form, the inertial contribution to $\langle \overline{f_D} \rangle_H / (\mu U_p)$ scales as $Re_p \langle \overline{u}''^2 \rangle_H / U_p^2$. White and Nepf (2003) found that $\langle \overline{u}''^2 \rangle / U_p^2$ increases with increasing ϕ in random arrays. Thus, the observed increase in α_1 with increasing ϕ is attributed in part to this trend, i.e., the increasing spatial variance of the time-averaged longitudinal velocity with increasing ϕ. A linear regression on α_1 and ϕ from the present study yields

$$\alpha_1 = (0.46 \pm 0.11) + (3.8 \pm 0.5)\phi \tag{13}$$

with $r=0.98$ ($n=5$). α_1 estimates based on Petryk's (1969) data and the isolated cylinder solution agree within uncertainty with Eq. (13), suggesting that this empirical expression is valid at ϕ below those investigated in the present study.

A similar ϕ dependence is not observed for α_0 in the present study. α_0 increases from 25 ± 12 at $\phi=0.091$ to 84 ± 14 at $\phi=0.15$, but remains constant within uncertainty for $\phi=0.15-0.35$ at $\alpha_0=83.8$, with a standard error of 0.6 ($n=4$). This suggests that viscous drag per cylinder length, $\alpha_0 \mu U_p$, remains independent of ϕ at $\phi \geq 0.15$. This behavior is inconsistent with the dependence predicted by scaling arguments. If we scale $-\partial \overline{u} / \partial n$ in Eq. (3) as $\langle \overline{u} \rangle / s$, where s=characteristic surface-to-surface separation between neighboring cylinders, the viscous contribution to $\langle \overline{f_D} \rangle_H$ scales as $\mu d \langle \overline{u} \rangle_H / s$. Accordingly, α_0 was expected to increase with increasing ϕ. It should be noted that α_0 is very sensitive to slight changes in the gradient of the line of regression, i.e., α_1. For example, a linear regression on interpolated values for the isolated cylinder yields $\alpha_0=114.6 \pm 0.1$ if applied over $Re_p=10^4-10^5$, instead of $\alpha_0=23.5 \pm 0.25$ obtained when the regression is applied over $Re_p=148-678$. In contrast, α_1 only changes from $0.5318 \pm 6 \times 10^{-4}$ to $0.5013 \pm 2 \times 10^{-6}$. This may explain the high values of α_0 associated with Petryk's (1969) measurements.

Fig. 5 illustrates C_D as a function of Re_p. C_D decreases as Re_p increases for all ϕ investigated. The data also demonstrate that C_D in a random array is larger than the isolated cylinder for $O(30) \leq Re_p \leq O(700)$ for $\phi \leq 0.35$. Results by Koch and Ladd (1997) and Petryk (1969) suggest that this functionality extends to all conditions they considered, as summarized in Table 2. In contrast, Nepf's (1999) measurements suggest that C_D is smaller than that of the isolated cylinder at higher Re_p.

Finally, note that while the numerical values measured in the present study only apply to randomly distributed smooth circular cylinders, the qualitative trends are expected to extend to plant stems of slightly different morphology and distribution. Specifically, C_D is expected to decrease as Re_p increases and increase as ϕ increases. For example, James et al.'s (2004) laboratory measurements of the depth-integrated drag exerted by an isolated *Phragmites australis* reed show that foliage enhances C_D in the range $Re_p=300-5{,}000$, where C_D was defined using the depth-integrated frontal area per unit depth as the characteristic plant width. Note that greater foliage implies larger ϕ. Similarly, Ayaz and Pedley (1999) and Stone and Shen (2002, Table 2) report increasing C_D with increasing ϕ in square and staggered arrays, respectively. Koch and Ladd (1997) also investigated square arrays at various orientation to the mean flow. Based on their tabulated results (Koch and Ladd 1997, Tables 1 and 2), C_D is higher at $\phi=0.4$ than 0.2 in each configuration for $50 < Re_p < 350$. These results suggest that the qualitative ϕ dependence may be independent of configuration.

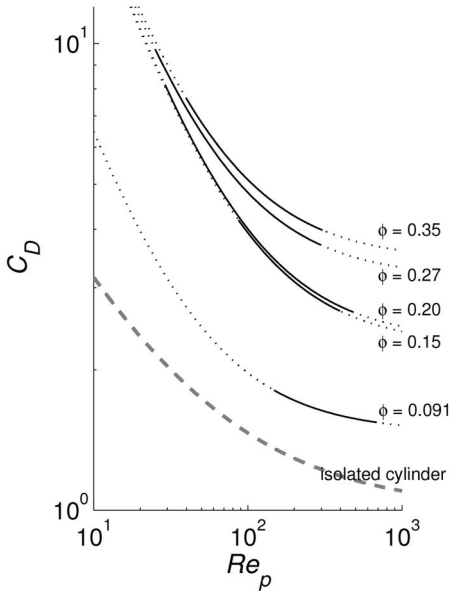

Fig. 5. C_D as a function of Re_p for $\phi=0.091$, 0.15, 0.20, 0.27, and 0.35 in the form of Eq. (5) with the fitted coefficients (solid lines) (Table 2). For reference, the fitted lines were extrapolated beyond the Re_p range of the data set (dotted line). Eq. (6) (dashed line) is also plotted.

Conclusions

Laboratory measurements of array drag were presented in the form of the array-averaged C_D and $\langle \overline{f_D} \rangle_H / (\mu U_p)$. Both C_D and $\langle \overline{f_D} \rangle_H / (\mu U_p)$ increase with ϕ. C_D monotonically decreases as Re_p increases. The Re_p dependence of $\langle \overline{f_D} \rangle_H / (\mu U_p)$ is consistent with Ergun's (1952) formulation, as was observed by Koch and Ladd (1997). Therefore, $\langle \overline{f_D} \rangle_H / (\mu U_p)$ and C_D for a given ϕ can be predicted by interpolating the values for α_0 and α_1 from Fig. 4 and Eq. (13), respectively, and applying them to Eqs. (4) and (5). However, these predictions are strictly valid only in the range $O(30) \leq Re_p \leq O(700)$. In particular, it should be noted that Nepf (1999) reports the opposite ϕ dependence of C_D at $Re_p > 1{,}000$. Additional measurements are required to determine if our results can be extrapolated to higher Re_p. Similarly, the Re_p dependence changes as Re_p approaches 0. Koch and Ladd (1997) show for $\phi=0.40$ that the drag exhibits a quadratic Re_p dependence at $0 < Re_p \leq 5$ and that Eq. (4) with coefficients as summarized in Table 2 underestimates $\langle \overline{f_D} \rangle_H / (\mu U_p)$ at $Re_p < 1$ (Koch and Ladd 1997, Fig. 23). Because experimental constraints on L restricted the analysis to high $Re_p (\geq 25)$, as discussed earlier, we could not capture the expected change in the Re_p dependence in the present study.

Acknowledgments

This material is based on work supported by National Science Foundation Grant No. EAR-0509658 and EAR-6895392. Any opinions, conclusions, or recommendations expressed in this material are those of the writers and do not necessarily reflect the views of the National Science Foundation. The writers thank undergraduate students Lucy L. Wu and Sheung Yan Sueann Lee for their assistance with the experiments and Brian L. White for providing unpublished ADV measurements from his Master's thesis

(White 2002). The writers also thank the three anonymous reviewers and the associate editor for their comments on the manuscript.

Notation

The following symbols are used in this paper:

C_D = temporally and spatially averaged drag coefficient, as defined in Eq. (1);
d = cylinder diameter or plant width;
$(dV/dz)_j$ = gradient of the linear regression of the calibration data for the jth gauge;
$\langle \overline{f_D} \rangle$ = mean drag per depth per cylinder at the local depth;
f_i = ith component of the net hydrodynamic force per unit mass of fluid acting on S_c, as defined in Eq. (3);
g_i = ith component of gravitational acceleration $(g_1=0, g_2=0, g_3=-g)$;
H = local, instantaneous water depth;
$\langle \bar{H} \rangle_L$ = mean of $\langle \bar{H} \rangle$ calculated from the upstream and the downstream gauges, with flow;
$\bar{H}_j$ = time-averaged water depth at the jth gauge, with flow;
H_{SWL} = still water depth;
L = longitudinal distance between upstream and downstream surface displacement gauges;
m = number of cylinders per unit horizontal area of array (including the area occupied by cylinders);
$\mathbf{n}$ = unit normal vector on S_c pointing out of the control volume V_f;
n = number of data points applied to a linear regression;
n_M = Manning's coefficient;
p = local, instantaneous pressure;
Q = volumetric flow rate;
R = hydraulic radius;
Re_p = cylinder Reynolds number ($\equiv U_p d/\nu$ or $\equiv \langle \bar{u} \rangle d/\nu$);
r = correlation coefficient;
S_c = all cylinder surfaces that intersect V_f;
s = characteristic surface-to-surface separation between neighboring cylinders;
t = time;
U_p = temporally and cross-sectionally averaged pore velocity;
V_f = fluid volume over which governing equations are averaged;
V_{f_j} = time-averaged voltage recorded from the jth gauge, with flow;
V_{0_j} = time-averaged reference voltage measurement for the jth gauge in still water;
$\mathbf{v} \equiv (u,v,w) \equiv (u_1,u_2,u_3)$ = local, instantaneous fluid velocity vector;
W = width of working section of laboratory flume;
$\mathbf{x} \equiv (x,y,z) \equiv (x_1,x_2,x_3)$ = Cartesian coordinates aligned with the mean flow, perpendicular to the mean flow in the horizontal plane, and perpendicular to the horizontal bed, respectively;
α_0 = empirical coefficient in Eqs. (4) and (5);
α_1 = empirical coefficient in Eqs. (4) and (5);
η = temporally and spatially averaged free surface displacement from the still water level;
η_j = time-averaged free surface displacement measured by the jth gauge, with flow;
μ = fluid viscosity;
ν = kinematic viscosity;
ρ = fluid density;
ϕ = solid volume fraction;
$\overline{\ }$ = time-averaging operation over an interval much longer than the time scales for turbulent fluctuations and vortex shedding;
$'$ = instantaneous deviations from the local time average;
$\overline{\ }''$ = local deviations of the time average from the spatial average;
$\langle\ \rangle$ = spatial-averaging operation over V_f; and
$\langle\ \rangle_H$ = spatial-averaging operation over V_f and over the water column.

References

Ayaz, F., and Pedley, T. J. (1999). "Flow through and particle interception by an infinite array of closely-spaced circular cylinders." *Eur. J. Mech. B/Fluids*, 18(2), 173–196.

Blevins, R. D. (2005). "Forces on and stability of a cylinder in a wake." *J. Offshore Mech. Arct. Eng.*, 127(1), 39–45.

Ergun, S. (1952). "Fluid flow through packed columns." *Chem. Eng. Prog.*, 48(2), 89–94.

Finnigan, J. (2000). "Turbulence in plant canopies." *Annu. Rev. Fluid Mech.*, 32, 519–571.

Finnigan, J. J. (1985). "Turbulent transport in flexible plant canopies." *The forest-atmosphere interaction*, B. A. Hutchison and B. B. Hicks, eds., Reidel, Dordrecht, Holland, 443–480.

Furukawa, K., Wolanski, E., and Mueller, H. (1997). "Currents and sediment transport in mangrove forests." *Estuarine Coastal Shelf Sci.*, 44(3), 301–310.

James, C. S., Birkhead, A. L., Jordanova, A. A., and O'Sullivan, J. J. (2004). "Flow resistance of emergent vegetation." *J. Hydraul. Res.*, 42(4), 390–398.

Kaimal, J. C., and Finnigan, J. J. (1994). *Atmospheric boundary layer flows. Their structure and measurement*, Oxford University Press, New York.

Knight, R. L., Kadlec, R. H., and Ohlendorf, H. M. (1999). "The use of treatment wetlands for petroleum industry effluents." *Environ. Sci. Technol.*, 33(7), 973–980.

Kobashi, D., and Mazda, Y. (2005). "Tidal flow in riverine-type mangroves." *Wetlands Ecology and Management*, 13(6), 615–619.

Koch, D. L., and Ladd, A. J. C. (1997). "Moderate Reynolds number flows through periodic and random arrays of aligned cylinders." *J. Fluid Mech.*, 349, 31–66.

Lee, J. K., Roig, L. C., Jenter, H. L., and Visser, H. M. (2004). "Drag coefficients for modeling flow through emergent vegetation in the Florida Everglades." *Ecol. Eng.*, 22(4), 237–248.

Leonard, L. A., and Luther, M. E. (1995). "Flow hydrodynamics in tidal marsh canopies." *Limnol. Oceanogr.*, 40(8), 1474–1484.

López, F., and García, M. (1998). "Open-channel flow through simulated vegetation: Suspended sediment transport modeling." *Water Resour. Res.*, 34(9), 2341–2352.

Mazda, Y., Wolanski, E., King, B., Sase, A., Ohtsuka, D., and Magi, M. (1997). "Drag force due to vegetation in mangrove swamps." *Mangroves and Salt Marshes*, 1(3), 193–199.

Nepf, H. M. (1999). "Drag, turbulence, and diffusion in flow through

emergent vegetation." *Water Resour. Res.*, 35(2), 479–489.
Nepf, H. M., Mugnier, C. G., and Zavistoski, R. A. (1997). "The effects of vegetation on longitudinal dispersion." *Estuarine Coastal Shelf Sci.*, 44(6), 675–684.
Petryk, S. (1969). "Drag on cylinders in open channel flow." Ph.D. thesis, Colorado State Univ., Fort Collins, Colo.
Poggi, D., Katul, G. G., and Albertson, J. D. (2004). "A note on the contribution of dispersive fluxes to momentum transfer within canopies." *Boundary-Layer Meteorol.*, 111(3), 615–621.
Serra, T., Fernando, H. J. S., and Rodriguez, R. V. (2004). "Effects of emergent vegetation on lateral diffusion in wetlands." *Water Res.*, 38(1), 139–147.
Stone, B. M., and Shen, H. T. (2002). "Hydraulic resistance of flow in channels with cylindrical roughness." *J. Hydraul. Eng.*, 128(5), 500–506.
Taylor, J. R. (1997). *An introduction to error analysis. The study of uncertainties in physical measurements*, 2nd Ed., University Science Books, Sausalito, Calif.
Tsujimoto, T., Shimizu, Y., Kitamura, T., and Okada, T. (1992). "Turbulent open-channel flow over bed covered by rigid vegetation." *J. Hydrosci. Hydr. Eng.*, 10(2), 13–25.
Valiela, I., Teal, J., and Deuser, W. (1978). "The nature of growth forms in the salt marsh grass *Spartina alterniflora*." *Am. Nat.*, 112(985), 461–470.
White, B. L. (2002). "Transport in random cylinder arrays: A model for aquatic canopies." Master's thesis, Massachusetts Institute of Technology, Cambridge, Mass.
White, B. L., and Nepf, H. M. (2003). "Scalar transport in random cylinder arrays at moderate Reynolds number." *J. Fluid Mech.*, 487, 43–79.
White, F. M. (1991). *Viscous fluid flow*, 2nd Ed., McGraw-Hill, New York.
Wu, F.-C., Shen, H. W., and Chou, Y.-J. (1999). "Variation of roughness coefficients for unsubmerged and submerged vegetation." *J. Hydraul. Eng.*, 125(9), 934–942.
Zdravkovich, M. M., and Pridden, D. L. (1977). "Interference between two circular cylinders; series of unexpected discontinuities." *J. Industrial Aerodynamics*, 2, 255–270.